Self-Assembled platinum nanoparticles into heavily fluorinated templates: reactive gas effect on the morphology

ARTICLE *in* NEW JOURNAL OF CHEMISTRY · APRIL 2009

Impact Factor: 3.09 · DOI: 10.1039/b822575c

8 AUTHORS, INCLUDING:

Bruno Chaudret
French National Centre for Scientific Resea…
278 PUBLICATIONS **9,243** CITATIONS
SEE PROFILE

Karine Philippot
French National Centre for Scientific Resea…
148 PUBLICATIONS **3,489** CITATIONS
SEE PROFILE

Yannick Guari
French National Centre for Scientific Resea…
131 PUBLICATIONS **2,461** CITATIONS
SEE PROFILE

Pierre Lecante
French National Centre for Scientific Resea…
126 PUBLICATIONS **3,096** CITATIONS
SEE PROFILE

Self-assembled platinum nanoparticles into heavily fluorinated templates: reactive gas effect on the morphology†‡

Mar Tristany,[abc] Marcial Moreno-Mañas,§[a] Roser Pleixats,*[a] Bruno Chaudret,[bc] Karine Philippot,*[bc] Yannick Guari,[d] Victor Matsura[d] and Pierre Lecante[e]

Received (in Montpellier, France) 16th December 2008, Accepted 3rd March 2009
First published as an Advance Article on the web 23rd March 2009
DOI: 10.1039/b822575c

The synthesis of platinum(0) nanoparticles by decomposition of $Pt_2(dba)_3$ under a dihydrogen or CO atmosphere and in the presence of heavily fluorinated stabilizers is described. Several techniques were used for the characterization of the obtained nanomaterials (TEM, HREM, WAXS and SEM-FEG) that organize into spherical or elongated superstructures made of small individual nanoparticles (*ca.* 2.5 nm).

Introduction

Much effort has been devoted in the past decade to the synthesis and the characterization of transition-metal nanoparticles (NPs). This interest comes from their small size and their particular electronic properties that lead to applications in various fields.[1] Different approaches have been reported for their preparation.[1,2] Among them the organometallic approach is now well-known and gives rise to well-controlled nanoparticles with tunable size, morphology and surface state.[3] Beside the mode of synthesis, the protecting agent used is also a key parameter: it prevents agglomeration and coalescence by forming a protective surrounding shell around the particles and thus allows stable and well-defined nanostructures to be obtained. Depending on the nature of the protecting agent, different types of stabilization exist:[1e] (1) electrostatic (surface adsorbed ions), (2) steric (large adsorbed molecules such as polymers or oligomers) and (3) electrosteric (ionic surfactants). An "entrapment" mechanism is also considered for block copolymers, cyclodextrins or dendrimers. Finally, the use of coordinating ligands (thiols, amines, phosphines *etc.*) has been strongly developed during the past years because of their ability to both allow coordination at the particle surfaces and produce steric hindrance around the particles, in particular when they contain long alkyl chains.[3] They are considered as "electrosteric" type stabilizers.[1e] For catalytic investigations in biphasic media, various heavily fluorinated compounds have also been tested as protecting agents for the synthesis of metal nanoparticles following various synthetic pathways.[4] Some of us have succeeded in the synthesis of small size fluorous-phase soluble ruthenium(0) and platinum(0) NPs following the organometallic approach in the presence of fluorinated compounds.[5] The stabilization effect of fluorous compounds on metal nanoparticles is not very clear. Whereas fluorous polymers[6] or fluorous dendrimers[7] are usually considered as entrapment-type stabilizers, stabilization by discrete fluorous compounds deserves some analysis because perfluoroalkanes are both hydrophobic and oleophobic.[8] The mechanism of stabilization by solid fluorous compounds possessing weakly coordinating functional groups, or no functional groups at all basically consists of entrapment of the NPs in the crystal lattice of the fluorous compound.[4e] Attractive forces between the negative peripheries of the perfluorinated chains and residual positive charges on the surface of the NPs could be responsible for this type of stabilization.[4e] Such an observation has also been reported for metal oxide NPs stabilized by perfluorinated alkanes (n-$C_{12}F_{26}$ and n-$C_{20}F_{42}$).[9] Other heavily fluorinated stabilizing compounds possessing appropriate functional groups are supposed to stabilize metal nanoparticles *via* the more classical electrostatic and/or steric mechanisms.[10–12]

The synthesis of Ru[5a] and Pt[5b] nanoparticles through the organometallic approach, gave rise to very nice superstructures composed of individual nanoparticles. The formation of these superstructures was explained by a phase-segregation phenomenon taking place in the reaction medium due to the low solubility of the fluorinated ligands in the solvent (THF). This hypothesis was supported by SEM-FEG observations that showed the tendency of the free ligand to self-organize in the reaction mixture.[5b] In addition, small angle X-ray scattering (SAXS) measurements confirmed the presence of nanoparticles organized into superstructures. However, there is a great difference between the results obtained with ruthenium and those obtained with platinum. This difference concerns the morphology of the

[a] *Department of Chemistry, Universitat Autònoma de Barcelona, Cerdanyola, 08193-Barcelona, Spain. E-mail: roser.pleixats@uab.cat; Fax: +34 935811265; Tel: +34 935812067*
[b] *CNRS, LCC (Laboratoire de Chimie de Coordination), 205 route de Narbonne, F-31077-Toulouse, France E-mail: karine.philippot@lcc-toulouse.fr; Fax: +33 561553003*
[c] *Université de Toulouse, UPS, INPT, LCC, F-31077-Toulouse, France*
[d] *Institut Charles Gerhardt, Chimie Moléculaire et Organisation du Solide, CNRS, UMR 5253, Université de Montpellier II, 34095 Montpellier Cedex 05, France*
[e] *Centre d'Elaboration des Matériaux et d'Etudes Structurales du CNRS, 29 rue Jeanne Marvig, BP4347-Toulouse Cedex 04, France*
† Dedicated to Prof. Josep Font at the occasion of his 70th birthday.
‡ Electronic supplementary information (ESI) available: Electron diffraction (S1) and wide angle X-ray scattering (WAXS) (S2). See DOI: 10.1039/b822575c
§ Deceased on 20th February 2006.

superstructures: spherical superstructures were observed with Ru but elongated ones (rods and wires) were obtained with Pt. This was particularly marked with perfluorinated aniline as a ligand, for which a trend to form spherical aggregates had been observed with ruthenium while nanorods and nanowires were formed with platinum. As the reaction conditions were not exactly the same for the two metallic systems, this led us to study their influence. The main difference being the reactive gas used for the precursor decomposition (H_2 for ruthenium and CO for platinum), we pursued our investigations by decomposing the $Pt_2(dba)_3$ (dba = dibenzylideneacetone) precursor under both dihydrogen and carbon monoxide atmospheres in the presence of discrete heavily fluorinated ligands to shed some light on the reactive gas and/or ligand influences on the superstructures' morphology. The obtained results are hereafter described.

Results and discussion

The synthesis of Pt NPs was achieved through decomposition at room temperature of the organometallic complex $Pt_2(dba)_3$ under dihydrogen (3 bar; Table 1) or carbon monoxide (1 bar; Table 2) and in the presence of heavily fluorinated ligands **L** (Scheme 1). Various experiments were carried out by changing the reaction conditions such as the solvent and the ligand : metal ratio, leading to different samples.

$Pt_2(dba)_3$ decomposition under H_2

Firstly, a series of experiments were carried out using dihydrogen as a decomposition gas. The first attempt was performed with aniline **L1** in 1,1,2-trichloro-1,2,2-trifluoroethane (CFC-113) as the solvent to enhance the ligand solubility, working with a **L1**/Pt molar ratio of 0.7. This experiment yielded amorphous nanoparticulate material (Table 1, **Pt1[L1]H_2**).

Then we moved to THF as solvent using two different molar ratios **L1**/Pt of 0.7 and 1.4 (Table 1, **Pt2[L1]H_2** and **Pt3[L1]H_2**). For these two cases, the THF colloidal media were not homogeneous. Suspensions and irregular aggregates of nanoparticles were observed by transmission electron microscopy (TEM) after redispersion of the black precipitates in CFC-113. The low stability of the NPs and their agglomeration can be explained by the low nucleophilic or coordinating character of aniline **L1** because of the combined effect of the perfluorinated chains electron-withdrawing nature and steric hindrance.

Therefore, we tested the aliphatic amine **L2** in which isolation of the amino group from the fluorous chain by methylene groups permits the retention of some coordinating power. In addition, no steric effects are present. Better results, *i.e.* homogeneous suspensions without precipitate, were obtained with this ligand in THF with molar ratios 1.4 and 2.8 (Table 1, **Pt4[L2]H_2** and **Pt5[L2]H_2**). TEM analysis showed the presence of spherical aggregates, the diameter of which is centered around 46–50 nm (Fig. 1 and 2).

In both **Pt4[L2]H_2** and **Pt5[L2]H_2** cases, HREM micrographs (Fig. 3 and 4) revealed that these aggregates are superstructures containing individual and small nanoparticles with an estimated mean size of 2.5 nm. As previously observed for ruthenium nanoparticles with the same ligand,[5a] we believe these superstructures result from a phase segregation phenomenon in the reaction mixture due to the low solubility of the fluorinated ligand in THF. Such phase segregation leads to the formation of a micelle type structure inside of which the metal precursor is confined. Thus, the decomposition of the precursor under dihydrogen pressure takes place inside the micelles that limit the nanoparticles' dispersion thanks to their embedding in the ligand coating.

Addition of pentane induced NP precipitation from the THF suspension. Redispersion of the solid in CFC-113 did not cause disruption of the nanoparticles' organization within the spherical superstructures. This behaviour is different from that observed for Ru superstructures: the precipitation by pentane addition had led to disruption of the spherical organization which was not recovered by further dispersion in CFC-113. This shows that the superstructures are more stable in the case of platinum.

Electron diffraction (ED) (Fig. S1‡) and wide-angle X-ray (WAXS) experiments (Fig. S2‡) confirmed the presence of face centered cubic (fcc) platinum(0) as usually observed.

A better idea of the macroscopic organization of the nanomaterials **Pt4[L2]H_2** and **Pt5[L2]H_2** was obtained by SEM-FEG analysis (Fig. 5). It appears clearly that the synthesized nanomaterials are formed of spherical superstructures that are more or less regular and made of individual platinum nanoparticles. Finally, elemental analysis (ICP) showed the presence of high percentages of Pt (76.1 and 64.5%) in the final nanomaterials.

From the two amine ligands tested (**L1** and **L2**), the aliphatic fluorous amine **L2** appears as the best stabilizer for the preparation of Pt(0) NPs by decomposition of $Pt_2(dba)_3$ with dihydrogen. Nevertheless, it seems that we are in the

Table 1 Platinum nanoparticles stabilized by fluorous compounds **L** obtained under dihydrogen

Material[a]	Ratio L/Pt[b]	Solvent	Morphology
Pt1[L1]H_2	0.7	CFC-113	Amorphous material constituted of NPs
Pt2[L1]H_2	0.7	THF	Irregular aggregates of NPs
Pt3[L1]H_2	1.4	THF	Irregular aggregates of NPs
Pt4[L2]H_2	1.4	THF	2.5 nm NPs aggregated in spheres of 46 nm. Fig. 1 and 3
Pt5[L2]H_2	2.8	THF	2.4 nm NPs aggregated in spheres of 50 nm. Fig. 2 and 4
Pt6[L3]H_2	6.8	THF	Ill-defined and strongly agglomerated NPs

[a] All reactions were performed at room temperature for 20 h unless otherwise stated and the morphology of the materials was determined by transmission electron microscopy (TEM) or scanning electronic microscopy with a field emission gun (SEM-FEG) from a drop of the crude colloidal THF solution (see experimental) unless otherwise stated. [b] Molar ratio taking into account the real Pt amount on the precursor determined by elemental analysis.

Table 2 Platinum nanoparticles stabilized by fluorous compounds **L** obtained under carbon monoxide

Material[a]	Ratio L/Pt[b]	Solvent	Morphology
Pt7[L1]CO	0.7	THF	Nice rods and nanowires made of individual NPs. Very dense nanomaterials (from ref. 5*b*)
Pt8[L1]CO	1.4	THF	
Pt9[L2]CO	0.7	THF	Nanorods (a.r. = 3.7), not well-defined, made of individual *ca.* 1.7 nm NPs. Fig. 6
Pt10[L2]CO	1.4	THF	Nanowires (a.r. = 26.7), not well-defined, made of individual *ca.* 1.4 nm NPs. Fig. 7

[a] All reactions were performed at room temperature for 20 h unless otherwise stated and the morphology of the materials was determined by transmission electron microscopy (TEM) or scanning electronic microscopy with a field emission gun (SEM-FEG) from a drop of the crude colloidal THF solution (see experimental) unless otherwise stated. [b] Molar ratio corrected taking into account the real Pt amount on the precursor determined by elemental analysis.

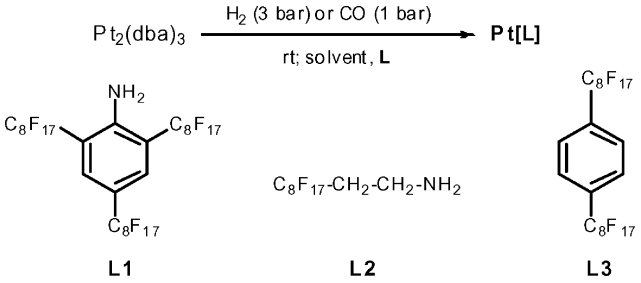

Scheme 1 Fluorinated stabilizers and synthesis of Pt NPs.

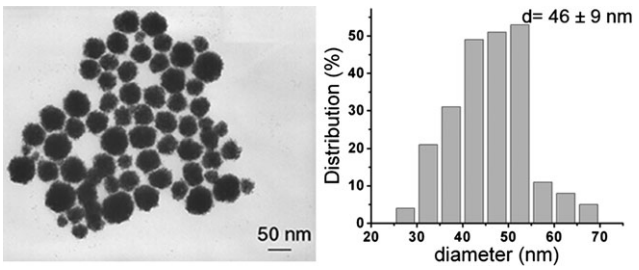

Fig. 1 TEM image of sample **Pt4[L2]H_2** and corresponding size histogram (d = mean diameter of the particles).

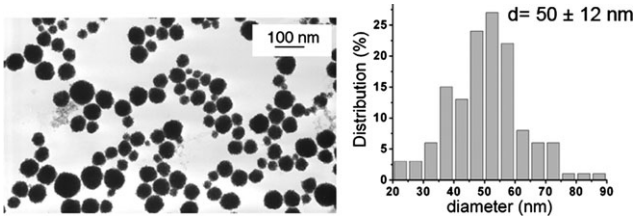

Fig. 2 TEM image of sample **Pt5[L2]H_2** and corresponding size histogram (d = mean diameter of the particles).

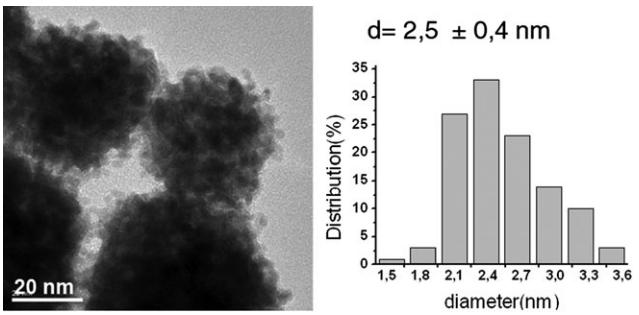

Fig. 3 HREM image of Pt NPs obtained for the molar ratio **L2**/Pt = 1.4 (**Pt4[L2]H_2**) and corresponding size histogram (d = mean diameter of the particles).

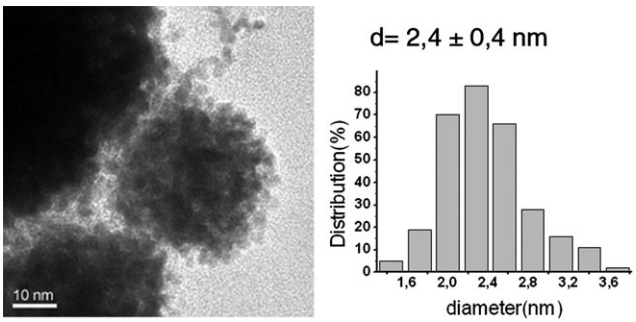

Fig. 4 HREM image of Pt NPs obtained for the molar ratio **L2**/Pt = 2.8 (**Pt5[L2]H_2**) and corresponding size histogram (d = mean diameter of the particles).

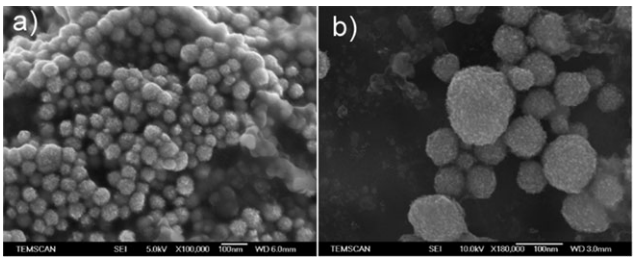

Fig. 5 SEM-FEG images of the crude THF suspension of colloids obtained (a) for the molar ratio **L2**/Pt = 1.4 (**Pt4[L2]H_2**) and (b) for the molar ratio **L2**/Pt = 2.8 (**Pt5[L2]H_2**).

presence of complex systems. Beside the formation of micelles in the reaction medium, leading to the NPs embedding in the ligand matrix, we cannot exclude, even if probably very weak, the possibility of the fluorous amine to act as a coordinating molecule at the NP surfaces. This would reinforce the NPs' stabilization and avoid their coalescence inside the micelles, and would then explain the formation of aggregates of individual nanoparticles. To try to shed some light on this hypothesis, novel syntheses were carried out in the presence of a fluorous ligand without amine function, **L3**. The structure of this ligand allows a comparison with the amine **L1**, for which irregular superstructures were observed. At previously used **L** : Pt ratios, no stabilization could be obtained with this ligand and precipitates were always observed. At higher ratio, that is for **L3**/Pt = 6.8 (Table 1, **Pt6[L3]H_2**), a nanoparticulate material could be obtained but the NPs appeared not well-defined, strongly agglomerated and without any tendency to organize. These later results confirm that long chain fluorous ligands can act as stabilizers for the synthesis of

NPs (*via* an entrapment effect) and secondly the importance of the amine function for a more efficient stabilization *via* an interaction with the particles' surfaces. Due to their low solubility in THF, the alkyl fluorous amines seem to induce organization into micelles in the reaction medium and the formation of platinum superstructures. This organization is favoured when the ligand concentration increases giving rise to a better confinement of the particles. These superstructures were not destroyed after isolation and redispersion in CFC-113 showing their high stability. The organization into spherical micelles may be reinforced through hydrogen bonding between amine groups and THF molecules or 1,5-diphenyl-3-pentanol (that comes from hydrogenation of dba molecules of the platinum precursor).

$Pt_2(dba)_3$ decomposition under CO

When we compare our previous results obtained with the same aniline **L1** but from decomposition of $Pt_2(dba)_3$ under CO instead of H_2,[5b] there is a great shape difference for the obtained superstructures. Under CO, very regular and elongated superstructures (nanorods or nanowires) made of individual nanoparticles were observed (**Pt7[L1]CO** and **Pt8[L1]CO**, Table 2), in particular at high ligand concentration.

The formation of the elongated superstructures containing individual NPs was previously explained by: (1) the organization of the fluorous aniline in the reaction medium which is favoured at high concentration and (2) the role of CO which coordinates at the particle surfaces and allows the stabilization of small NPs. Thus, it appeared that clearly it was necessary to distinguish between the role of the ligands and the role of the reactive gas on the morphology of the superstructures. For that purpose, we carried out a decomposition of the platinum precursor in the presence of the fluorinated alkylamine **L2** under CO (Table 2) and compared the results with those obtained previously with **L1**.[5b] Under these conditions, we also obtained elongated

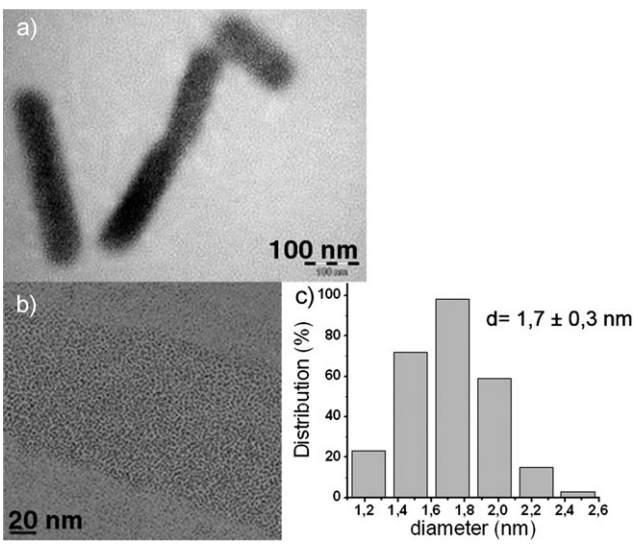

Fig. 6 TEM image (a) and HREM image (b) of elongated Pt superstructures obtained for the molar ratio **L2**/Pt = 0.7 (**Pt9[L2]CO**) and (c) corresponding size histogram (d = mean diameter of the particles).

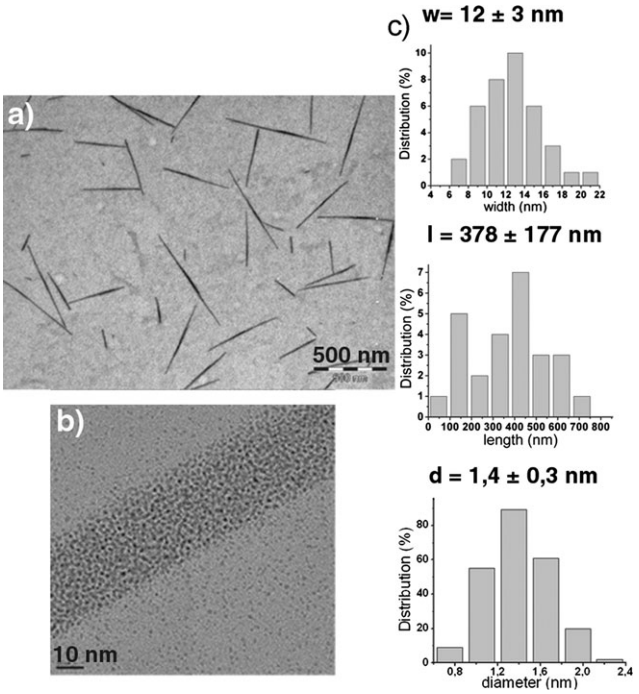

Fig. 7 TEM image (a) and HREM image (b) of elongated Pt superstructures obtained for the molar ratio **L2**/Pt = 1.4 (**Pt10[L2]CO**) and (c) size histograms (w = nanorods width; l = nanorods length; d = mean diameter of the particles).

superstructures for materials **Pt9[L2]CO** (Fig. 6) and **Pt10[L2]CO** (Fig. 7). In these materials the distance between the nanoparticles is estimated at 1.24 ± 0.28 nm and 1.22 ± 0.30 nm, respectively, and seems to correspond to interdigitated ligands.

In addition, as previously observed with **L1**, when the **L2**/Pt ratio increases the superstructures are more regular in size and display a higher aspect ratio. Nevertheless, these superstructures appear smaller and less thick than with **L1**. There is thus a template effect of the stabilizer on the superstructures' morphology control and aniline **L1** seems to induce a more rigid organization in the reaction medium. However, these experiments also confirm that the morphology of the platinum superstructures strongly depends on the reactive gas: while H_2 allows the formation of spherical superstructures, CO directs towards the formation of elongated ones. The hypotheses are the following: (1) a H_2 atmosphere leads to the formation of surface hydrides, as previously observed in the case of ruthenium; this would favour weak ligand interaction with the particles' surfaces and the tendency for the NPs to agglomerate into spherical superstructures because of a low stabilization effect. (2) CO coordination at the particles' surfaces provides their stabilization, thus disfavouring ligand interaction with the particle surface and promoting ligand self-organization and the formation of rods, as independently observed in the absence of metal particles. In the literature, the self assembly of platinum nanoparticles into nanofibers has already been observed in the presence of CO and swollen liquid crystals[13] or hexadecylamine[14] as a soft template.

Conclusions

This study provides evidence that fluorinated ligands can act as weak stabilizers for the synthesis of metal nanoparticles. Different results were obtained in the preparation of Pt(0) nanoparticles depending on the reaction conditions, and most particularly the reactive gas (Scheme 2).

First of all, under a dihydrogen atmosphere, taking into account that fluorinated ligands without functional groups such as **L3** are efficient only at high ligand/metal ratio, they can be considered as ''entrapment'' type stabilizers. Further, the presence of functional groups such as amines on the fluorinated ligands reinforce their stabilization effects, giving rise to small and individual nanoparticles. In this case there is probably a weak but effective coordination of the amine at the particle surfaces that allows a better stabilization leading us to think that they can also be considered as ''electrosteric'' type stabilizers like traditional ligands. This is particularly marked for the alkylfluorinated amine **L2**. Finally, at high concentration, fluorinated compounds allow the formation of organized nanoparticles into spherical superstructures. They self-assemble in the reaction medium and behave as organic soft templates able to favour directed assembly of the particles into spherical superstructures.

Secondly, when CO is used as the decomposition gas, CO molecules coordinate at the particle surfaces. This reinforces the nanoparticles' stabilization. In these conditions, the role of the fluorinated amines as coordinating agents at the particle surfaces may be secondary and they can fully act as a soft organic template giving rise to nice elongated superstructures. This tendency is particularly strong with the aniline ligand **L1** for which the superstructures are more regular and more dense leading us to think that NPs are better confined.

In summary, these results evidence the interest of the joint use of heavily fluorinated compounds as stabilizers and organometallic precursors as a metal source, to induce organization of metal nanoparticles into superstructures. They also show that an adequate choice of the reaction conditions, the reactive gas being a key parameter, allows the morphology of the obtained superstructures to be tuned. This could be useful to obtain composite nanomaterials of various morphologies whose organization could have an influence on their properties for a targeted application.

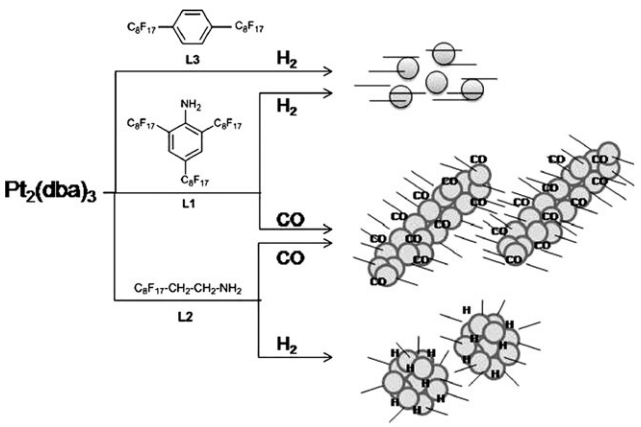

Scheme 2 Various superstructures observed depending on the ligand and the reaction conditions.

Experimental

General procedures and reagents

Compound **L3** (mp 103–104 °C, lit.[15] mp 106 °C) was prepared by the method of McLoughlin and Thrower.[16] Aniline **L1** was obtained by perfluoroalkylation of aniline[17] and amine **L2** by the method of Reyé *et al.*[18] The precursor $Pt_2(dba)_3$ was synthesized by a method adapted from the literature.[19] The amount of Pt was checked by elemental analysis. The synthesis of $Pt_2(dba)_3$ and all operations concerning nanoparticles were carried out in Schlenk or Fischer-Porter glassware under argon or in a glove-box. K_2PtCl_4 (from Alfa Aesar) was used without purification. Solvents were dried and distilled before use: CFC-113 by trap to trap, THF over sodium benzophenone and pentane over calcium hydride. All reagents and solvents were degassed before use by means of three freeze–pump–thaw cycles.

IR spectra (KBr pellets) were recorded on a Perkin-Elmer Spectrometer GX (FT-IR). Samples for TEM/HREM and SEM-FEG analyses were prepared by slow evaporation of a drop of crude colloidal solution deposited under argon onto holey carbon-covered copper grids. In some cases grids were prepared after dispersion in THF or CFC-113 of the isolated nanomaterial after precipitation with pentane. The TEM and SEM-FEG analyses were performed at the ''Service Commun de Microscopie Electronique de l'Université Paul Sabatier'' (TEMSCAN). TEM images were obtained using a JEOL 200CX-T electron microscope operating at 200 kV with resolution point of 4.5 Å. SEM-FEG experiments were performed on a CM20 STEM-FEG (field emission gun) microscope. HREM observations were carried out at the ''Servei de Microscòpia de la UAB'' with a JEOL JEM 2010 electron microscope working at 200 kV with a resolution point of 2.5 Å. The size distributions were determined through a manual analysis of enlarged micrographs by measuring *ca.* 300 particles on a given grid to obtain a statistical size distribution and a mean diameter. Data collection for the wide-angle X-ray scattering (WAXS) were performed on small amounts of powder at the CEMES-CNRS (Toulouse). All samples were sealed in 1 mm diameter Lindemann glass capillaries. The measurements of the X-ray intensity scattered by the samples irradiated with graphite-monochromatized molybdenum K_α (0.071069 nm) radiation were performed using a dedicated two-axis diffractometer. Radial distribution functions (RDF) were obtained after Fourier transformation of the reduced intensity functions. The crystalline structure was determined through comparison with theoretical fcc Pt.

Preparation of nanoparticles

The procedure for the preparation of platinum nanoparticles is hereafter illustrated through the case of sample **Pt4[L2]H_2** (see Table 1, entry 4).

$Pt_2(dba)_3$ (154 mg, 0.141 mmol) was introduced in a Fischer-Porter bottle under an argon atmosphere and a

vacuum was made. 1*H*,1*H*,2*H*,2*H*-tetrahydroperfluorodecylamine (134.8 mg, 0.291 mmol) was dissolved in THF (40 mL) and was degassed by freeze–pump cycles. The resultant solution was transferred in the Fischer-Porter flask. The bottle was pressurized under 3 bar of dihydrogen and the mixture was left stirring at room temperature. After 20 h, a black suspension was obtained. After the elimination of excess dihydrogen the volume of the suspension was reduced to 1/3 and it was added to 20 mL of cold pentane. The resulting dark mixture was cooled at 193 K and any dark solid was precipitated. It was evaporated until it was dry, and 20 mL of pentane was added. The mixture was cooled at 193 K and a dark solid precipitated. It was washed with pentane (2 × 20 mL) and finally dried, giving rise to 46.2 mg of a black solid. IR (KBr) ν: 2918, 1201, 1146 cm^{-1}. EA: 4.16/3.91% C, 0.0/0.0% H, 0.24/0.30% N, 5.39% F, 75.90/76.30% Pt. ΣEA: 85.8%. Estimated molecular formula: $Pt_{561}(\mathbf{L2})_{24}(THF)_x$ TEM from the initial THF suspension: spherical aggregates of 46 ± 9 nm constituted by small nanoparticles (Fig. 1); HREM from the initial THF suspension: spherical aggregates constituted by individual and well-defined small nanoparticles 2.51 ± 0.35 nm (113 particles) (Fig. 3). Yield: 64%. WAXS analysis: metallic fcc platinum nanoparticles >4 nm (Fig. S2‡). SEM-FEG from black solid redispersed in CCl_2F–$CClF_2$: irregular aggregations of spherical aggregates of little nanoparticles (Fig. 5a).

Acknowledgements

Financial support from MEC of Spain (Projects CTQ2005-04968/BQU and CTQ2006-04204/BQU, predoctoral scholarship to M. T.), Generalitat de Catalunya (Projects SGR2005-00305 and PICS 2003-2), from CNRS of France (Project PICS no. 2428) and Consolider Ingenio 2010 (CSD2007-00006) is gratefully acknowledged. The authors are also indebted to V. Collière (TEMSCAN-UPS) and O. Castells (SM-UAB) for electron microscopy.

References

1 (*a*) *Clusters and Colloids. From Theory to Applications*, ed. G. Schmid, VCH, Weinheim, 1994; *Nanoparticles. From Theory to Applications*, ed. G. Schmid, Wiley-VCH, Weinheim, 2004; (*b*) K. J. Klabunde and C. Mohs, in *Chemistry of Advanced Materials. An Overview*, ed. L. V. Interrante and M. J. Hampden-Smith, Wiley-VCH, New York, 1998, ch. 7; (*c*) *Nanoscale Materials in Chemistry*, ed. K. J. Klabunde, Wiley-Interscience, New York, 2001; (*d*) *Metal Nanoparticles. Synthesis, Characterization, and Applications*, ed. D. L. Feldheim and C. A. Foss, Jr, Marcel Dekker, New York, 2002; (*e*) A. Roucoux, J. Schulz and H. Patin, *Chem. Rev*., 2002, **102**, 3757–3778; (*f*) M. Moreno-Mañas and R. Pleixats, *Acc. Chem. Res*., 2003, **36**, 638–643; (*g*) A. Roucoux, *Top. Organomet. Chem*., 2005, **16**, 261–279; (*h*) M. A. Malik and P. O'Brien, *Top. Organomet. Chem*., 2005, **9**, 173–204; (*i*) D. Astruc, F. Lu and J. R. Aranzaes, *Angew. Chem., Int. Ed*., 2005, **44**, 7852–7872; (*j*) A. Roucoux and K. Philippot, in *Handbook of Homogeneous Hydrogenations*, ed. J. G. de Vries and C. J. Elsevier, Wiley-VCH, Weinheim, 2007, vol. 9, pp. 217–255.

2 B. L. Cushing, V. L. Kolesnichenko and C. J. O'Connor, *Chem. Rev*., 2004, **104**, 3893–3946.

3 (*a*) K. Philippot and B. Chaudret, *C. R. Chim*., 2003, **6**, 1019–1034; (*b*) B. Chaudret, *C. R. Phys*., 2005, **6**, 117–131; (*c*) B. Chaudret, *Top. Organomet. Chem*., 2005, **16**, 233–259; (*d*) K. Philippot and B. Chaudret, in *Comprehensive Organometallic Chemistry III*, ed. R. H. Crabtree and M. P. Mingos, Elsevier, Amsterdam, 2007, vol. 12, ch. 12.03, pp. 71–99.

4 (*a*) E. B. Zuckerman, K. J. Klabunde, B. J. Olivier and C. M. Sorensen, *Chem. Mater*., 1989, **1**, 12–14; (*b*) K. J. Klabunde, G. Youngers, E. J. Zuckerman, B. J. Tan, S. Antrim and P. M. Sherwood, *Eur. J. Solid State Inorg. Chem*., 1992, **29**, 227–260; (*c*) M. Moreno-Mañas, R. Pleixats and S. Villarroya, *Organometallics*, 2001, **20**, 4524–4528; (*d*) M. Moreno-Mañas, R. Pleixats and S. Villarroya, *Chem. Commun*., 2002, 60–61; (*e*) M. Tristany, J. Courmarcel, P. Dieudonné, M. Moreno-Mañas, R. Pleixats, A. Rimola, M. Sodupe and S. Villarroya, *Chem. Mater*., 2006, **18**, 716–722; (*f*) M. Moreno-Mañas, R. Pleixats and M. Tristany, *J. Fluorine Chem*., 2005, **126**, 1435–1438; (*g*) A. Serra-Muns, R. Soler, E. Badetti, P. de Mendoza, M. Moreno-Mañas, R. Pleixats, R. M. Sebastián and A. Vallribera, *New J. Chem*., 2006, **30**, 1584–1594; (*h*) S. Niembro, A. Vallribera and M. Moreno-Mañas, *New J. Chem*., 2008, **32**, 94–98.

5 (*a*) M. Tristany, B. Chaudret, P. Dieudonné, Y. Guari, P. Lecante, V. Matsura, M. Moreno-Mañas, K. Philippot and R. Pleixats, *Adv. Funct. Mater*., 2006, **16**, 2008–2015; (*b*) M. Tristany, M. Moreno-Mañas, R. Pleixats, B. Chaudret, K. Philippot, P. Dieudonné and P. Lecante, *J. Mater. Chem*., 2008, **18**, 660–666.

6 For a review, see: (*a*) M. Moreno-Mañas and R. Pleixats, in *Handbook of Fluorous Chemistry*, ed. J. A. Gladysz, D. P. Curran and I. T. Horváth, Wiley-VCH, Weinheim, 2004, ch. 12.2, pp. 491–507. For ruthenium nanoparticles entrapped in Nafion, see: (*b*) O. Solorza-Feria and S. Durón, *Int. J. Hydrogen Energy*, 2002, **27**, 451–455.

7 (*a*) R. M. Crooks, M. Zhao, L. Sun, V. Chechik and L. K. Yeung, *Acc. Chem. Res*., 2001, **34**, 181–190; (*b*) R. M. Crooks, B. I. Lemon III, L. Sun, L. K. Yeung and M. Zhao, *Top. Curr. Chem*., 2001, **212**, 81–135.

8 *Organofluorine Chemistry. Principles and Commercial Applications*, ed. R. E. Banks, B. E. Smart and J. C. Tatlow, Plenum, New York, 1994.

9 (*a*) I. Lamparth, D. V. Szabó and D. Vollath, *Macromol. Symp*., 2002, **181**, 107–112; (*b*) D. V. Szabó, I. Lamparth and D. Vollath, *Macromol. Symp*., 2002, **181**, 393–398; (*c*) D. Vollath, I. Lamparth and D. V. Szabó, *Mater. Res. Soc. Symp. Proc*., 2002, **703**, 303–308.

10 (*a*) P. S. Shah, J. D. Holmes, R. C. Doty, K. P. Johnston and B. A. Korgel, *J. Am. Chem. Soc*., 2000, **122**, 4245–4246; (*b*) T. Yonezawa, S. Onoue and N. Kimizuka, *Adv. Mater*., 2001, **13**, 140–142; (*c*) T. Yonezawa, S. Onoue and N. Kimizuka, *Langmuir*, 2001, **17**, 2291–2293.

11 S. J. Lee, S. W. Han and K. Kim, *Chem. Commun*., 2002, 442–443.

12 (*a*) M. Ji, X. Chen, C. M. Wai and J. L. Fulton, *J. Am. Chem. Soc*., 1999, **121**, 2631–2632; (*b*) H. Ohde, F. Hunt and C. M. Wai, *Chem. Mater*., 2001, **13**, 4130–4135; (*c*) H. Ohde, C. M. Wai, H. Kim, J. Kim and M. Ohde, *J. Am. Chem. Soc*., 2002, **124**, 4540–4541.

13 G. Surendran, G. Apostolescu, M. Tokumoto, E. Prouzet, L. Ramos, P. Beaunier, P. J. Kooyman, A. Etcheberry and H. Remita, *Small*, 2005, **1**, 964–967.

14 E. Ramirez, L. Eradès, K. Philippot, P. Lecante and B. Chaudret, *Adv. Funct. Mater*., 2007, **17**, 2219–2228.

15 A. Schulte, V. M. Hallmark, R. Twieg, K. Song and J. F. Rabolt, *Macromolecules*, 1991, **24**, 3901–3905.

16 V. C. R. McLoughlin and J. Thrower, *Tetrahedron*, 1969, **25**, 5921–5940.

17 M. Moreno-Mañas, R. Pleixats and S. Villarroya, *Synlett*, 1999, 1996–1998.

18 O. Porcherie, Y. Guari and C. Reyé, *New J. Chem*., 2005, **29**, 538–543.

19 K. Moseley and P. M. Maitlis, *J. Chem. Soc. D*, 1971, 982–983.

